Experimental study of the electrical conductivity of strongly coupled copper plasmas

Alan W. DeSilva* and H.-J. Kunze
Experimentalphysik V, Ruhr-Universität Bochum, Bochum, Germany
(Received 10 November 1993)

The electrical conductivity of copper has been measured in the range of densities 0.3–3 gm/cm^3 and in the temperature range from 8 000 to 30 000 K. Copper wires were vaporized in glass capillaries, and the conductivity measured in the 1-μs interval after vaporization began, and before the tube disintegrated. Measured conductivities are compared with several theoretical models.

PACS number(s): 52.25.Fi, 52.20.Fs, 52.80.Qj

I. INTRODUCTION

Plasmas may be characterized by the coupling constant $\Gamma = Z^2e^2/akT$, as strongly coupled, or nonideal, when Γ is of order unity or greater. [$a = (3/4\pi n)^{1/3}$, is the ion-sphere radius.] Γ represents the ratio of mean potential energy to mean kinetic energy per particle, and is closely related to the plasma parameter $\Lambda = 1/nD^3$, where D is the Debye length. Plasmas having $\Gamma > 1$ are encountered in nature in the cores of dwarf stars and of giant gaseous planets, in the solar photosphere, and probably in the core plasma of a lightning stroke.

In the laboratory, such plasmas occur in arcs, railguns, and in laser-compressed plasmas created in inertial confinement fusion experiments. To date, much of what is known about these interesting plasmas has been obtained from theory, supplemented by Monte Carlo computer modeling studies.

Experimentally, such plasmas are difficult to create in the laboratory, since large Γ implies high density and low temperature. A minimum temperature is necessary to ionize the gas, and even at the lowest temperatures satisfying the condition of large Γ, the density must be so high that the plasma is at a very high pressure, which renders magnetic confinement impracticable. Diagnosis by the ordinary techniques of spectroscopy is also difficult, since at the densities encountered these plasmas are optically thick so that the only radiation to be seen comes from their surface.

An exception to the conditions outlined above is the case of cryogenic pure ion or electron plasmas confined in magnetic fields. These have been studied by laser cooling of ions [1] or synchrotron radiation cooling of electrons [2] in a magnetic trap, and in groups of ions circulating in a storage ring [3]. The total number of such confined particles in such experiments is relatively small, however, and true three-dimensional plasma effects have so far eluded study.

Exploding wire plasmas have been widely studied, and strongly coupled plasmas are produced in these discharges. However, in the case of unconfined wire explosions, the density of the resulting plasma is ill defined, making precise measurement of the properties of the dense plasma difficult. In addition, instabilities tend to produce axially nonuniform plasmas, making interpretation of conductivity measurements uncertain [4].

Wire explosions confined by glass capillaries [5], water [6,7], and plastics [8] have been reported, but these studies generally focused on the later phases of the discharge after considerable expansion of the initial current channel had occurred.

Strongly coupled plasmas created by high current discharges in alkali metals and noble gases in capillaries have been studied [9–11] for plasma densities in the range of 10^{20} cm^{-3}, and a measurement of the electrical conductivity of the plasma resulting from evaporating material from the inner wall of a capillary in polyethylene has been reported [12].

We have studied the electrical conductivity of strongly coupled plasmas having coupling constants ranging up to about 70, created by rapid vaporization of copper wires in glass capillaries.

The capillary confines the plasma in a uniform and measurable volume for a short time, during which it is possible to make accurate measurements of the conductivity, density and input energy, and to make good estimates of the plasma temperature and pressure.

II. EXPERIMENT

Copper wires with diameters of 125 or 250 μm were inserted into glass capillaries 22 mm in length, having inner diameters ranging from 300 to 890 μm. The capillaries were clamped between electrodes as indicated in Fig. 1, and a rapidly rising current from a capacitor bank vaporized the wire and heated the resultant gas to the plasma state. The capacitor bank consisted of two 1.93-μF capacitors in parallel, charged to 6–16 kV, and was switched by means of a pressurized spark gap switch. The inductance of the bank was 133 nH, and the load (wire) inductance was typically about 40 nH. Current was measured by means of a Rogowski coil mounted on the grounded side of the capillary support and voltage by a resistive voltage divider connected to the high voltage

*Permanent address: Institute for Plasma Research, University of Maryland, College Park, MD 20742.

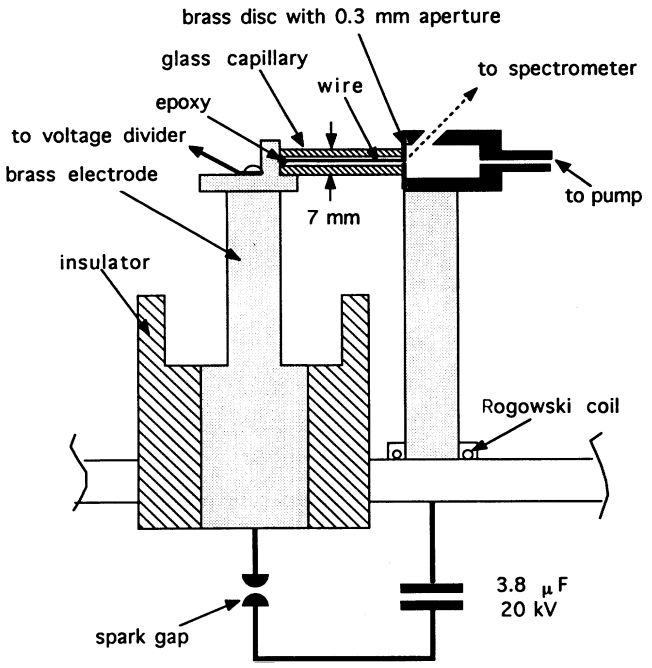

FIG. 1. Schematic of capillary discharge assembly. The small chamber at the right of the capillary is evacuated for a shot.

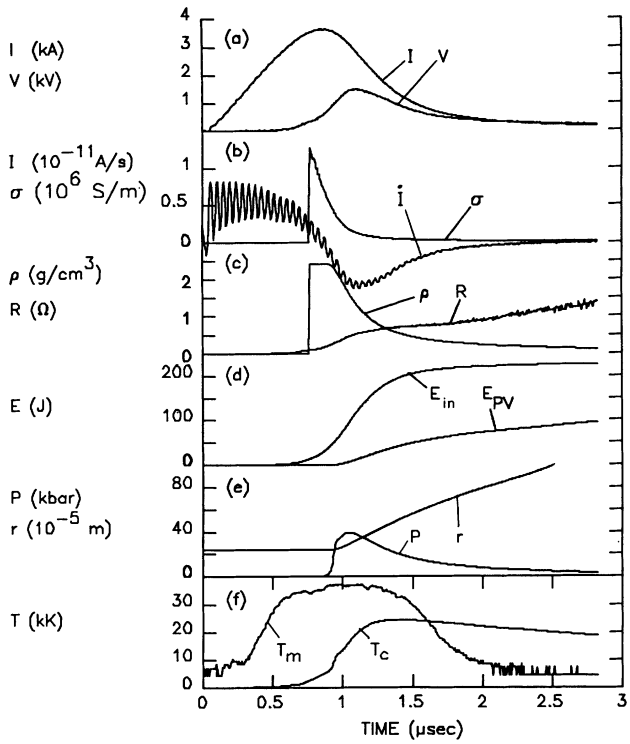

FIG. 2. Time record of a typical discharge. (a) I: current; V: voltage corrected for inductance effects, (b) $\dot{I}$: derivative of current; σ: conductivity in siemens/m, (c) ρ: density; R: resistance of copper column, (d) E_{in}: energy into wire; E_{PV}: energy into work compressing glass, (e) P: plasma pressure from the model; r: capillary inner radius: (f) T_m: temperature from radiation intensity; T_c: temperature from the model. The high frequency ringing evident on the dI/dt trace in (b) is due to the external circuit and has little effect on the plasma.

electrode near the capillary (Fig. 1).

The voltage consists of an inductive component $LdI/dt + IdL/dt$, and a resistive component IR. It is the latter that we need in order to deduce the plasma conductivity. The term due to changing inductance arises from the change in diameter of the current-carrying column from that of the wire to that of the plasma filling the inner diameter of the capillary, and to expansion of the capillary inner diameter. In most cases, this term is negligible. The term LdI/dt consists of the inductance of the current column plus the inductance of the grounded support rod that holds the capillary. dI/dt was determined from the Rogowski loop, and the inductance was determined as that necessary to satisfy $V = LdI/dt$ in the first few hundred nanoseconds, when the wire resistivity and current are both low enough so that the IR term is negligible. Figure 2(a) shows typical time records of the current and voltage.

As the wire vaporizes, its cross section diminishes and consequently its resistance rises. At the same time, the density of the vapor rises rapidly due to confinement by the glass wall, and the gas passes smoothly into the plasma phase with no evidence of the "restrike" phenomenon that has been reported in the case of unconfined wire explosions [13].

At the densities encountered in these measurements, the optical depth τ of the plasma column is high in the visible range and $\tau \approx 1$ is reached at a depth of only a few micrometers so the plasma radiates as a blackbody at a temperature characteristic of the surface plasma. A measurement of the radiation emitted through the wall of the capillary will therefore yield a temperature characteristic of the plasma near the cold glass boundary, and would not necessarily be characteristic of the core temperature.

A somewhat more characteristic temperature should be measurable from the radiation emitted by the plume of plasma ejected from one of the open ends of the capillary. Accordingly, observations were made of the spectrum of radiation emitted both through the capillary walls, and from the plasma plume.

III. DATA ANALYSIS AND MODELING

The plasma resistance is easily found from the current and resistive voltage drop, but in order to determine the conductivity it is necessary to know the plasma column diameter. Initially, (after the wire has fully vaporized), this is the diameter of the capillary, but, owing to the high pressure of the plasma, the glass tube wall is compressed, and the inner diameter grows with time. This pressure pulse generates a shock wave in the tube wall, which propagates outward at a speed of about 4.2 mm/μs. The inner wall diameter grows at a much lower rate, owing to the very low compressibility of glass. Figure 2(e) shows the growth of the inner tube radius, from a model discussed in the next section. At the time the shock reaches the outer wall of the tube, about 700 nsec later, the outer wall spalls off, with a velocity of twice

the particle velocity behind the shock wave [14]. Figure 3 shows a typical streak photograph of the tube, in which the expansion of the outer wall is evident. For this picture, the tube was back lighted by an argon flash lamp, so it is seen in silhouette. The shock itself is invisible in the photograph, but its arrival at the outer wall of the tube is evident as the point where the outer wall begins to expand.

The bright feature expanding outward from the center has a velocity close to that of the shock. It is thought to be due to light which originates in the cylindrical plasma at the center of the tube, and subsequently scatters from fractured glass in the region close behind the shock. It is this light that prevents us from making direct optical measurements of the plasma column diameter, and which forces us to turn to a dynamic model of the pressure pulse in glass to deduce the inner wall diameter.

The glass is compressed in the radial direction, but as the inner radius increases, the inner wall must come under tension in the azimuthal direction, which would cause radial fractures to appear as soon as the tension exceeds the tensile strength of the glass. In some experiments, a small section of the tube wall was prevented from exploding by a massive, close-fitting disk surrounding the tube. In such a case, the glass remaining inside the disk after a shot was observed to be intensely fractured, with the fracture lines running radially. Light from the plasma is thought to scatter from this fracture zone, the radius of which increases as the shock moves outward. It is evident in Fig. 3 that light begins appearing from the outer wall diameter of the tube slightly before the arrival there of the expanding light feature. This is the time that the shock reaches the outer wall, and causes it to shatter, now scattering light directly from the outer wall.

All measurements are made in the short time interval from the start of pressure increase as the wire vaporizes, until the shock has reached the outer tube wall and reflected back to the inner wall. The pressure pulse rises to its peak typically in a period of about 200 nsec, and it takes about 1.4 μs for the reflected shock to return to the inner wall.

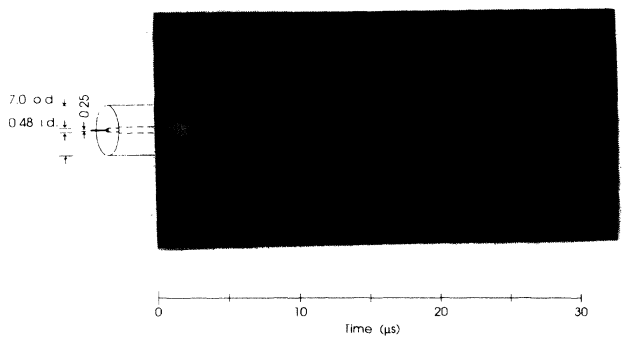

FIG. 3. Streak photograph of a discharge, with the slit oriented perpendicular to the the tube axis and positioned at the middle of the tube. The tube was backlighted and is seen in silhouette. Dimensions in mm of the tube and wire are shown on the left. See text for explanation of triangular bright feature shown on the left.

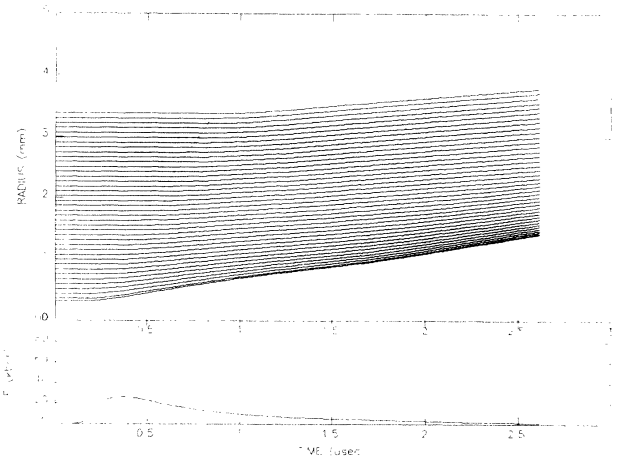

FIG. 4. Glass compression model code results. Plotted are the time histories of the 40 shells used to model the glass tube. A line has been drawn to indicate the shock wave locus. Below is the pressure profile used in this calculation.

IV. SHOCK MODEL

We have constructed a one-dimensional numerical model of the glass dynamics in which the glass tube is represented by 40 concentric mass shells, which interact through the bulk compressibility. The behavior of glass to high pressure shocks has been studied by Wackerle [15], and the behavior of quartz by Fuller and Price [16]. These works show that the Hugoniot for glass is nearly linear for pressures up to 200 kbar. Wackerle shows that for pressures of from zero to 70 kbar, the Hugoniot for one type of glass has a slight negative curvature, which leads to an instability in the shock propagation, causing there to be an initial step of low amplitude, followed by a sharp shock transition. The existence of such a double feature in the pressure profile would not be resolved in our measurements, which are made on the later time behavior of the ejected material, which is influenced only by the sharp shock. The pressure inside the tube is taken from the plasma model discussed in the next section. The glass compression model follows the position and velocity of each of the mass shells in time, and clearly shows the propagation of a shock wave initiated by the initial pressure rise (Fig. 4). The computer code was run with the assumption of zero tensile strength for the glass, so that when the shock reaches the outer wall, the material is ejected with a speed equal to twice that of the material just behind the shock when it reaches the wall. This velocity may be compared with the observed velocity deduced from streak photographs such as that shown in Fig. 3.

With help of this model, we can determine the inner wall diameter, which is taken to be the plasma column diameter, as a function of time.

V. PLASMA MODEL

The principal purpose of the plasma model is to produce an estimate of the plasma pressure, which is then

used in the glass compression model discussed above to determine the inner wall diameter.

We trace the time history of a typical discharge with help of a zero-dimensional numerical model of the plasma that takes as its input the energy input to the wire from the external circuit. We have available as recorded data the current through the wire $I(t)$ (recorded as the derivative dI/dt), and the voltage $V(t)$ across the wire, in 5-nsec steps. Starting from the wire at room temperature, the energy input is determined from the product I^2R, where R is the resistance of the wire, taken from published data of the resistivity of copper as a function of temperature [17,18]. At early times, the measured voltage across the wire is dominated by the inductive drop, and, although this can, in principle, be corrected for, the errors involved are so large that the use of computed resistivity is by far the most accurate way to determine the energy input. The rise in temperature of the wire is related to the energy input using tabulated data for the specific heat of copper [19], and melting of the wire is similarly accounted for using published data for the latent heat of fusion [20]. By the time the melting point is reached, the voltage across the wire has risen to a high enough level relative to the inductive voltage that the measured voltage may thenceforth be used to compute the energy input.

After the melting point is reached, a theoretical equation of state for copper is used to relate the energy input to the temperature and pressure. This equation was developed at the Lawrence Livermore Laboratory by piecing together six theoretical models covering various regions of parameter space [21]. The plasma parameters are modeled in time in the following manner: starting from an initial temperature, density and internal energy, at each time step the experimentally determined energy increment is added isochorically to determine a new pressure and temperature. The new pressure is then used in the glass shock model discussed above to advance the tube wall expansion, resulting in a new density. The equation of state tables are then used again to make an adiabatic expansion to the new density and temperature. At each succeeding step, the electrical input energy is reduced by the work done by the plasma on the tube wall. Thus in the model, each time step consists of an isochoric addition of energy followed by an adiabatic expansion. The pressure profile that results from such a calculation is shown in Fig. 2(e).

We check the results of this calculation by comparing the outer wall velocity observed on the streak images with that computed from the plasma and glass models. We also compare the measured temperature of the plume ejected from the end with the plasma model temperature.

VI. OBSERVATIONS

Light emitted through the tube walls becomes detectable at about the time the temperature reaches 5000 K. The observed onset of light corresponded well in time to the code calculations based on observed energy input and on the tabulated equation of state. The temperature deduced from the absolute intensity of this radiation, corrected for the increase in effective area due to scattering from fractured glass behind the shock, remained quite low in all observation conditions, due to the cooling effect of the tube wall and the very small optical depth of the dense plasma, never reaching above about 6000 K.

Temperatures were also deduced from the absolute intensity of radiation of the plume of plasma emerging from the end of the capillary. Measurements were made on the plume looking at 90° to the tube axis just outside the end of the capillary, as well as looking directly into the end of the tube. We also made measurements looking at the plume escaping into vacuum, rather than into atmospheric pressure air, at 90° and at 60° to the tube axis. These latter measurements were made to ensure that the intensity was not being influenced by radiation from the surrounding atmosphere. In all of these measurements, it was often observed that the onset of light occurred several hundred nanoseconds before the time light became measurable through the capillary walls. Framing camera pictures confirmed that sparking appeared in the region where the copper wire contacted the electrode at the onset of current flow. Shots made with the wires firmly clamped at the electrodes eliminated this early appearing light.

The spectrum of the plume was measured with a low dispersion spectrometer coupled to an optical multichannel analyzer in the range 250–600 nm. In the range 400–600 nm, the spectrum fits a blackbody continuum at the temperature deduced from an absolute measurement of the continuum at 450 nm. Below 400 nm, the observed spectrum is a continuum, punctuated by an occasional absorption line. It was not possible, however, to get a reliable calibration of the instrument in this region.

In the work reported here, the capillary was mounted so as to allow evacuation of its interior and of the region around one end (Fig. 1). Plasma escaping from that end into vacuum could be observed, without influence by the surrounding atmosphere. In order to make an electrical connection to the wire inside the capillary, a brass disk 500 μm in thickness, having a hole in its center 300 μm in diameter, was glued with epoxy to the end of the capillary, with care to keep the interior of the capillary free of epoxy . The copper wire was inserted from the opposite end until it contacted the disk, and the wire was then immobilized with a drop of epoxy which closed the open end so the tube could be evacuated. The disk sealed with an *o* ring against a small chamber which was evacuated, along with the inside of the capillary, before the shot, so that the plasma plume escaped into vacuum. It was viewed at an angle of 45° from the tube axis. The hole in the brass plate was focused on the entrance plane of a Jarrell-Ash $\frac{1}{4}$-m monochromator, and the slit masked so that it viewed only a rectangular region 30 μm by 130 μm positioned to view the plume just as it emerged from the hole. This arrangement did allow the sparking discussed above to occur where the wire contacted the disk, so the early appearing light was ignored. However, the ejected plasma later should dominate the radiation.

The plasma temperature was deduced from measurement of the absolute intensity of the radiation from the

plume in a band of 0.5-nm width, centered at 445 nm. A typical record is shown in Fig. 2(f). The region around 445 nm was determined to be free of observable absorption lines. Referring to Fig. 2(f), one can see that the radiation from the region viewed by the spectrometer rises immediately as current flows, showing that a spark occurs at the connection between wire and the brass electrode. The intensity of radiation from this spark cannot be taken as indicating the temperature of the wire. However, after the wire has fully vaporized, we assume that the radiation is characteristic of the interior plasma escaping through the aperture in the brass disk.

Typical plasma temperatures in the plume were about 8 000–30 000 K. This implies that the sound speed in the plasma should be of the order 1 mm/μs, and so one expects that a rarefaction wave will propagate into the open end of the tube as plasma is ejected there. Our measurements are all made within the first 1 μs after the plasma pressure rises, so the change in length of the plasma column is small enough that it may be neglected.

We find that the temperature deduced from the intensity of the plume corresponds well, generally within 30%, with that deduced from the numerical modeling. However, since the plume temperature is clearly not useful in the times earlier than that of full vaporization, we have chosen to present the data as functions of the computed temperature.

VII. RESULTS AND DISCUSSION

The radial expansion model discussed above is employed to determine the time behavior of the inner radius of the capillary, from which the cross-sectional area of the plasma is found. A check on the glass compression model is to compare its prediction for the outer wall velocity with that observed in the streak photographs. The outer wall velocity found from the model has been found to be sensitive to the peak pressure, and relatively insensitive to the integrated impulse given by the inner pressure. Comparing the observations with the model, we find that for almost all the cases studied, the model predicts outer wall velocities that are equal to those measured within experimental error, estimated at $\pm 20\%$. The exception is in the case of 125 μm diameter wires with high rate of energy input, for which the measured wall velocities are about twice those predicted by the model. In these cases, the streak photographs show irregularities indicating nonsymmetrical fracturing.

Figure 2 shows the time record of a single typical shot. Measured quantities in this record are the current and voltage, and the light intensity from which the temperature may be measured. The rest of the curves represent the output of the code. The current rises as a sinusoid in time, which would peak at about 1.5 μs in the absence of changes in the wire resistance. The wire begins to vaporize at about 800 nsec, and has completely vaporized by about 1 μs. At this time the pressure inside the tube [Fig. 2(e)] rises rapidly, and the voltage [Fig. 2(a)] also begins to rise as the resistance increases by about two orders of magnitude. The increasing pressure of the copper vapor causes the tube to begin to expand [Fig. 2(e)], causing the density to decrease [Fig. 2(c)]. The energy input to the copper column [Fig. 2(d)] also increases rapidly, while the work done in compressing the glass [Fig. 2(d)] increases more slowly. The conductivity [Fig. 2(b)] is high at the time vaporization begins, and drops rapidly, owing both to the rising temperature [Fig. 2(f)] and to the decreasing density.

The temperature deduced from the absolute intensity of the radiation from the plume escaping from the tube end [Fig. 2(f)] rises soon after the initiation of the current, and long before wire vaporization could begin. This is attributed to light originating in a spark forming at the connection between wire and electrode at the tube end. The contact resistance due to the spark has been shown to be negligible. Later in time, in this example, the radiation temperature is about 30% higher than that computed from the energy input, which is an atypically large discrepancy. The radiation temperature falls at about 1.5 μs, which coincides with the time that the tube has fully fractured and is now rapidly disintegrating. The computed model continues to assume confinement of the plasma, and is unrealistic after this time. In the following, we use data only from the time vaporization begins to 1-μs later.

With the cross-sectional area determined from the glass expansion model, the density and conductivity of the plasma are now easy to compute. In this, we assume that the original wire is fully vaporized and fills the capillary uniformly. We also assume that the radial fracturing of the glass discussed above creates a negligible additional volume for the plasma. In Figs. 5–7, we show the conductivity as a function of density for three temperatures (10 000, 20 000, 30 000 K). The temperatures are taken from the code calculations, as we believe these to be more accurate and reliable than those deduced from radiation intensity. Each point is from a different shot, taken at

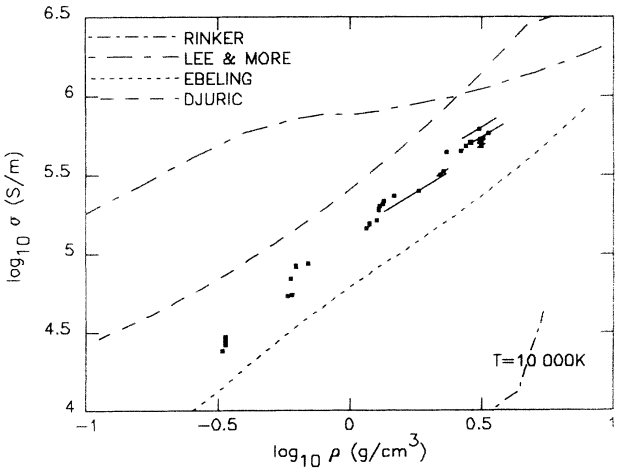

FIG. 5. Measured conductivity at a temperature of 10 000 K. Error bars indicate correlated uncertainty in the tube radius, and in some cases are smaller than the plot symbols. Also shown are theoretical results of Rinker (Ref. [23]), Ebeling *et al.* (Ref. [25]), Djurić *et al.* (Ref. [26]), and Lee and More (Ref. [24]) The theory of Djurić is for $Z = 1$.

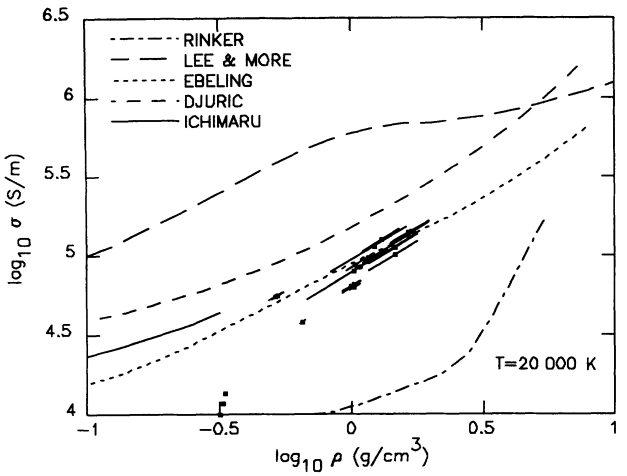

FIG. 6. As in Fig. 5, for 20 000 K. Theory of Ichimaru and Tanaka [Ref. 22], valid for $Z = 1$ and $\Gamma < 2$, is also shown.

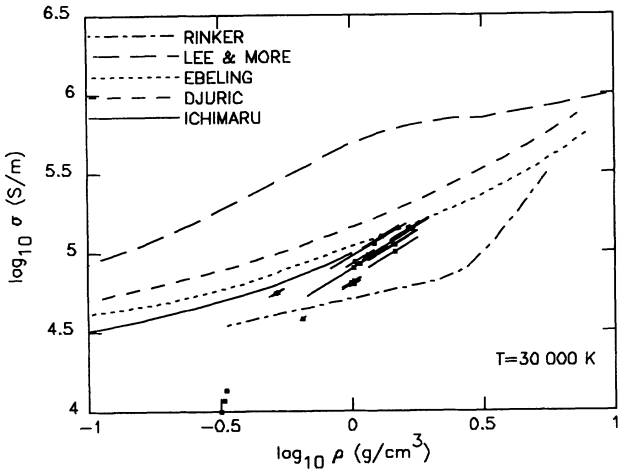

FIG. 7. As in Fig. 5, for 30 000 K.

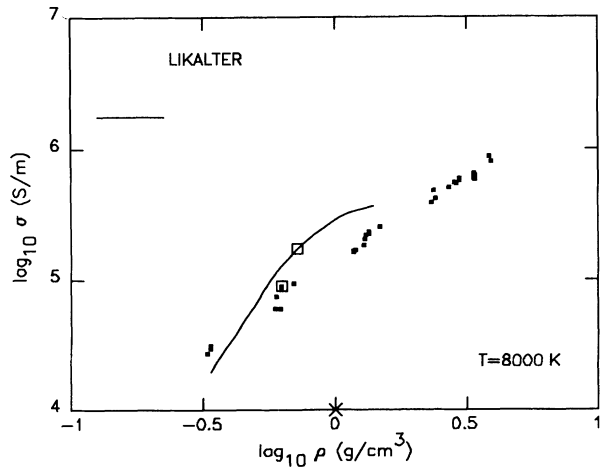

FIG. 8. The theory of Lik'alter (Ref. [27]), for a temperature of 7 600 K, with our results for 8 000 K.

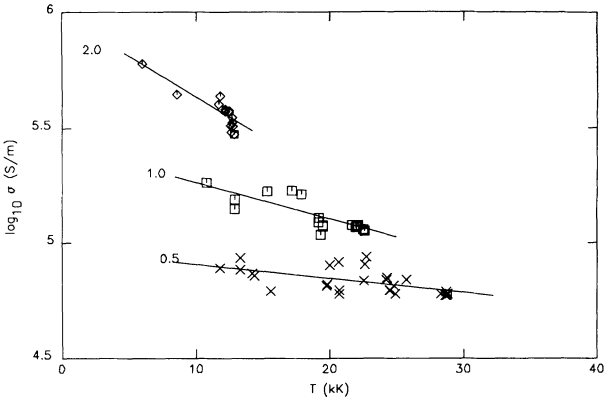

FIG. 9. Measured conductivity versus temperature for densities of 2.0, 1.0, 0.5 g/cm^3. Solid lines are linear least squares fits to the data.

the time the code shows the plasma passing through the selected temperature. Data are from 38 shots covering a variety of conditions, using capillaries varying from 300 μm in diameter to 890μm, and with wires of 125 and 250 μm diameter, and initial voltage on the capacitor bank varying from 6 to 16 kV. Error bars shown in the figures indicate uncertainty in the tube radius, which reflects as correlated errors in both the conductivity and density, hence the slanted error bars. The error in temperature is estimated at $\pm 30\%$, but this estimate is uncertain, as the temperature follows from many steps of integration over the equation of state tables, whose accuracy is not well known. Also shown are the predictions of theories

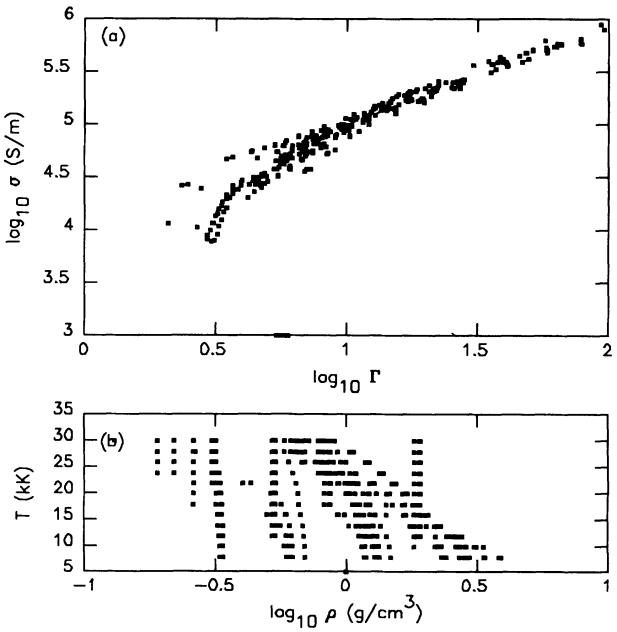

FIG. 10. (a) Measured conductivities for a wide range of densities and temperatures, plotted as a function of coupling parameter Γ. (b) Location in temperature and density space of the data entering into (a).

of Ichimaru and Tanaka [22], Rinker [23], Lee and More [24], Ebeling *et al.* [25], and Djuric *et al.* [26]. Lik'alter has considered specifically a copper plasma, but presents a prediction only for the critical temperature 7 600 K [27]. Figure 8 shows his theory, along with our data for 8 000 K.

From the same set of data, the temperature dependence of the conductivity for constant density may be extracted. Temperatures were noted for the times on each shot when the density passed through selected density. The results, for densities of 2.0, 1.0, and 0.5 g/cm^3 are shown in Fig. 9.

It is interesting to note that, when plotted versus coupling parameter Γ, the conductivity data collapse nearly to a line, at least for $\Gamma > 10$, suggesting that for large Γ, the conductivity is a function only of Γ. Figure 10(a) shows the data from 38 shots plotted as conductivity vs Γ. In Fig. 10(b), we plot the density versus temperature coordinates of the same data, indicating the range of parameter space covered. The value of Z used in determination of Γ for this figure was taken from a Thomas-Fermi approximation [28].

ACKNOWLEDGMENTS

This work was performed while one of us (A.W.D.) was a guest at the Ruhr-Universität Bochum, Germany, supported by the Deutsche Forschungsgemeinschaft, to which he gives grateful acknowledgment. Additional support came from the NSF. The authors are indebted to Dr. F. J. Rogers for making listings of the equation of state tables available, and to Dr. L. Jones, Dr. J. Benage, and Dr. S. Lyon for assistance in obtaining the relevant LANL SESAME tables. We also thank I. Krisch and R. Durand for assistance.

[1] S. L. Gilbert, J. J. Bollinger, and D. J. Wineland, Phys. Rev. Lett. **60**, 2022 (1988).
[2] T. M. O'Neil, P. G. Hjorth, B. Beck, J. Fajans, and J. H. Malmberg, in *Proceedings of Yamada Conference XXIV on Strongly Coupled Plasma Physics,* edited by S. Ichimaru (Yamada Science Foundation, Lake Yamanaka, Japan, 1990), pp. 313–324.
[3] R. W. Hasse and J. P. Schiffer, Ann. Phys. (NY) **203**, 419 (1990), and references therein.
[4] K. S. Fansler and D. D. Shear, in *Exploding Wires*, edited by W. G. Chace and H. K. Moore (Plenum Press, New York, 1959), Vol. 4, pp. 185-193.
[5] C. P. Nash, R. P. DeSieno, and C. W. Olsen, in Ref. [4], Vol. 3, pp. 231–246.
[6] R. R. Buntzen, in Ref. 4, Vol. 2, pp. 195–205.
[7] J. A. Kersavage, in Ref. 4, Vol. 2, pp. 225–233.
[8] I. M. Fyfe and R. R. Ensminger, in Ref. 4, Vol. 3, pp. 257-265. See also F. D. Bennett, Phys. Fluids **5**, 102 (1961).
[9] S. G. Barol'skii, N. V. Ermokhin, P. P. Kulik, and V. A. Ryabyi, High Temp. (USSR) **14**, 626 (1976).
[10] P. P. Kulik, E. K. Rozanov, and V. A. Ryabyi, High Temp. (USSR) **15**, 349 (1977).
[11] V. M. Adamyan, G. A. Gulyi, N. L. Pushek, P. D. Starchik, I. M. Tkachenko, and I. S. Shvets, High Temp. (USSR) **18**, 186 (1980).
[12] R. L. Shepherd, D. R. Kania, and L. A. Jones, Phys. Rev. Lett. **61**, 1278 (1988).
[13] See, e.g., R. J. Reithel, J. H. Blackburn, G. E. Seay, and S. Skolnick, in *Exploding Wires*, edited by W. G. Chace and H. K. Moore (Plenum Press, New York, 1959), Vol. 1, pp. 19–23, W. G. Chace and R. L. Morgan, *ibid.*, Vol. 1, pp. 59–72.
[14] J. M. Walsh and R. H. Christian, Phys. Rev. **97**, 1544 (1955).
[15] J. Wackerle, J. Appl. Phys. **33**, 922 (1962).
[16] P. J. A. Fuller and J. H. Price, Br. J. Appl. Phys. **15**, 751 (1964).
[17] M. J. Laubitz, Can. J. Phys. **45**, 3677 (1967).
[18] T. Iida and R. I. L. Guthrie, *The Physical Properties of Liquid Metals* (Clarendon Press, Oxford, 1988), p. 232.
[19] *Landolt-Börnstein Tables*, edited by K.-H. Hellwege and J. L. Olsen Landolt-Bornstein New Series, Group III, Vol. 15a (Springer-Verlag, Berlin, 1982), p. 31.
[20] *International Critical Tables*, edited by E. W. Washburn (McGraw-Hill, New York, 1926) p. 15.
[21] K. S. Trainor, J. Appl. Phys. **54**, 2372 (1983).
[22] S. Ichimaru and S. Tanaka, Phys. Rev. A **32**, 1790 (1985).
[23] G. A. Rinker, Phys. Rev. A **37**, 1284 (1988); **31**, 4207 (1985).
[24] Y. T. Lee and R. M. More, Phys. Fluids **27**, 1273 (1984).
[25] W. Ebeling, A. Förster, V. E. Fortov, V. K. Gryaznov, and A. Ya. Polishchuk, *Thermophysical Properties of Hot Dense Plasmas* (B. G. Teubner Verlagsgesellschaft, Stuttgart, 1991), Vol. 25, p. 274.
[26] Z. Djurić, A. A. Mihajlov, V. A. Nastasyuk, M. Popovic, and I. M. Tkachenko, Phys. Lett. A **155**, 415 (1991).
[27] A. A. Lik'alter, J. Phys. Cond. Matter **4**, 10 125 (1992).
[28] R. M. More, Adv. At. Mol. Phys. **21**, 305 (1985).

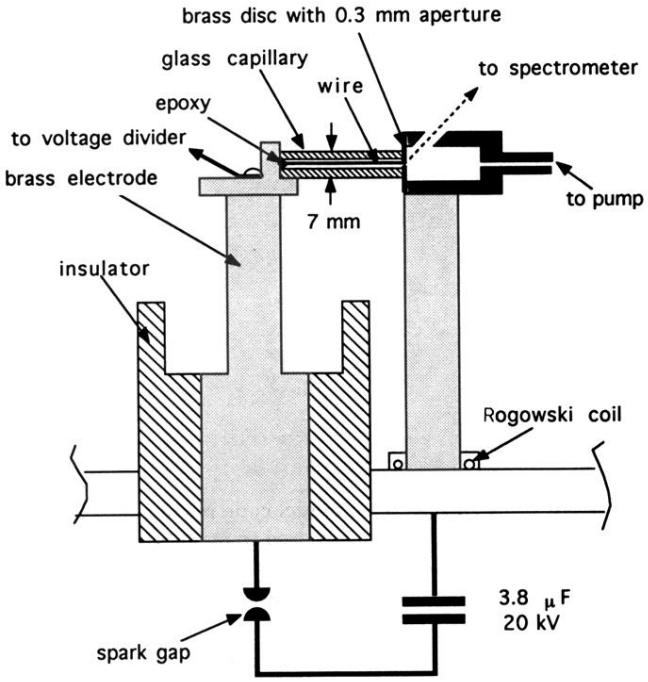

FIG. 1. Schematic of capillary discharge assembly. The small chamber at the right of the capillary is evacuated for a shot.

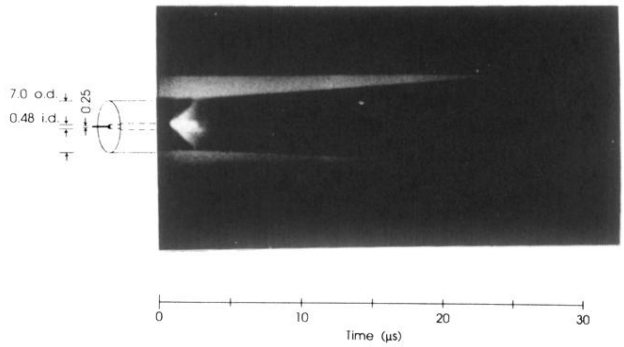

FIG. 3. Streak photograph of a discharge, with the slit oriented perpendicular to the the tube axis and positioned at the middle of the tube. The tube was backlighted and is seen in silhouette. Dimensions in mm of the tube and wire are shown on the left. See text for explanation of triangular bright feature shown on the left.